

Multicritical behavior of the fidelity susceptibility for the 2D quantum transverse-field XY model

Yoshihiro Nishiyama

Received: date / Accepted: date

Abstract The two-dimensional quantum XY model with a transverse magnetic field was investigated with the exact diagonalization method. Upon turning on the magnetic field h and the XY -plane anisotropy η , there appear a variety of phase boundaries, which meet at the multicritical point $(h, \eta) = (2, 0)$. We devote ourselves to the Ising-universality branch, placing an emphasis on the multicritical behavior. As a probe to detect the underlying phase transitions, we adopt the fidelity susceptibility χ_F . The fidelity susceptibility does not rely on any presumptions as to the order parameter involved. We made a finite-size-scaling analysis of χ_F for $\eta = 1$ (Ising limit), where a number of preceding results are available. Thereby, similar analyses with η scaled were carried out around the multicritical point. We found that the χ_F data are described by the crossover scaling theory. A comparison with the preceding studies of the multicriticality is made.

1 Introduction

For the quantum mechanical systems, the fidelity F is defined by the overlap

$$F = |\langle h|h + \Delta h \rangle|, \quad (1)$$

between the ground states with the proximate interaction parameters, h and $h + \Delta h$; here, the symbol $|h\rangle$ denotes the ground-state vector for the Hamiltonian with the interaction parameter h . The idea of fidelity was developed in the course of the study of the quantum dynamics [1, 2, 3, 4]. Meanwhile, it turned out that the fidelity is sensitive to the quantum phase transitions. Actually, the fidelity susceptibility

$$\chi_F = \frac{1}{N} \partial_{\Delta h}^2 F|_{\Delta h=0}, \quad (2)$$

Department of Physics, Faculty of Science, Okayama University, Okayama 700-8530, Japan

with the system size N exhibits a notable peak around the phase transition point [5, 6, 7, 8, 9]; see Refs. [10, 11] for a review. In fact, the fidelity susceptibility displays a pronounced peak as compared to that of the specific heat [12]. As would be apparent from the definition (2), the fidelity susceptibility is readily tractable with the exact diagonalization method. It has to be mentioned that the fidelity susceptibility is accessible via the quantum Monte Carlo method [12, 13, 14, 15] and the experimental observation [16, 17, 18] as well.

In this paper, we investigate the two-dimensional quantum XY model with a transverse magnetic field. Upon turning on the magnetic field h and the XY -plane anisotropy η , there appear a variety of phase boundaries, which merge at the multicritical point $(h, \eta) = (2, 0)$. We devote ourselves to the Ising-universality branch, aiming to reveal how the Ising-universality branch ends up at the XX -symmetric multicritical point. As a probe to detect the phase transitions, we adopt the fidelity susceptibility. The fidelity susceptibility is sensitive to both Ising- and XX -symmetric phase transitions, because it does not rely on any presumptions as to the order parameter involved. As a matter of fact, the similar approaches, namely, the fidelity-susceptibility-mediated analyses [19] of the multicriticality [20], have been made for the one-dimensional counterpart; see Refs. [21, 22, 23] for the information-theoretical approaches as well. In the present paper, stimulated by these recent developments, we apply the fidelity-susceptibility-mediated scheme to the case of two dimensions. Note that the one-dimensional XY model is exactly solvable [24, 25, 26], and the concerned singularities have been investigated in depth. On the contrary, such sophisticated techniques are not available in two dimensions, and the detail still remains an open issue.

To be specific, we present the Hamiltonian for the two-dimensional quantum XY model with a transverse magnetic field [27]

$$\mathcal{H} = -J \sum_{\langle ij \rangle} ((1 + \eta) S_i^x S_j^x + (1 - \eta) S_i^y S_j^y) - h \sum_{i=1}^N S_i^z. \quad (3)$$

Here, the quantum spin-1/2 operator \mathbf{S}_i is placed at each square-lattice point, $i = 1, 2, \dots, N$ ($N = L^2$). The summation, $\sum_{\langle ij \rangle}$, runs over all possible nearest-neighbor pairs, $\langle ij \rangle$; here, the periodic boundary condition is imposed. The coupling J denotes the nearest-neighbor ferromagnetic XY interaction, and it is regarded as the unit of energy throughout this study; namely, we set $J = 1$ hereafter. The parameter η denotes the XY -plane anisotropy, which interpolates the Ising ($\eta = 1$) and XX ($\eta = 0$) symmetric cases smoothly. The magnetic field h induces the phase transition between the ordered ($h < h_c(\eta)$) and disordered ($h > h_c(\eta)$) phases for respective η . This phase boundary $h_c(\eta)$ belongs to the Ising universality class [27]. A schematic phase diagram [27] for the model (3) is presented in Fig. 1. Within the semicircle (dashed), the correlation function gets modulated spatially, and along the line $\eta = 0$ (thick), the XX -ordered phase is realized eventually. Note that the nature of this XX -ordered phase differs significantly from that of the one-dimensional counterpart [19, 20, 21, 22, 23]. because the latter corresponds to the case of

Fig. 1 A schematic phase diagram for the two-dimensional quantum XY model with a transverse magnetic field (3) is presented. Here, the parameters, h and η , denote the transverse magnetic field and the XY -plane anisotropy, respectively. For $h > (<)h_c(\eta)$, the paramagnetic (Ising-ordered) phase extends. Within the semicircle (dashed), the correlation function gets modulated, and eventually, along the line $\eta = 0$ (thick), the XX order is realized. A topological index is specified to each phase surrounding the multicritical point $(h, \eta) = (2, 0)$ [28], suggesting a subtlety of this point.

the lower critical dimension (Tomonaga-Luttinger liquid), and the XX order develops only marginally. Noticeably enough, the phase boundaries in Fig. 1 meet at the multicritical point $(h, \eta) = (2, 0)$; actually, a topological-index is specified [28] to each regime surrounding the multicritical point. Thereby, there arises a problem how the Ising-universality branch $h_c(\eta)$ ends up at this XX -symmetric point; see Fig. 2. The exact diagonalization simulation [27] for the $N \leq 5 \times 5$ cluster indicates a “monotonous” [29] dependence of $h_c(\eta)$ on η . On the contrary, the spin-anisotropic-spherical-model analysis [29] revealed a reentrant behavior around the multicritical point, claiming that the simulation data [27] are “too few and too far apart from a final conclusion” [29]. The aim of this paper is to explore the multicriticality with the crossover scaling analysis of the fidelity susceptibility for the cluster with $N \leq 6 \times 6$ spins so as to estimate the crossover critical exponent ϕ quantitatively.

Upon applying a magnetic field h within the XX -symmetric sector $\eta = 0$, the magnetization saturates at the multicritical point, where a severe slowing down [30] affects the efficiency of the quantum Monte Carlo simulations. This point is characterized by an enhancement of the dynamical critical exponent $z = 2$ [31], for which an asymmetry between the real-space and imaginary-time subspaces emerges. Hence, special care has to be taken with the ratio between the real-space and imaginary-time system sizes, L and β , respectively, to carry out the scaling analysis properly. Because the exact diagonalization method admits us to access the ground state ($\beta \rightarrow \infty$) directly, it is free from such

Fig. 2 As to the Ising-universality branch $h_c(\eta)$ depicted in Fig. 1, the spin-anisotropic spherical model displays a reentrant behavior [29], whereas the exact diagonalization analysis for $N \leq 5 \times 5$ [27] suggests a “monotonous” [29] dependence on η . In this paper, based on the crossover scaling analysis for $N \leq 6 \times 6$, we estimate the crossover exponent ϕ quantitatively.

complications as to the size of β . Hence, we are able to concentrate only on the L -dependent behaviors as in the ordinary finite-size-scaling analyses.

We recollect a number of related studies [12, 27, 32, 33, 34, 35, 36] for the two-dimensional quantum XY (Ising) model (3) in Table 1. As indicated, in order to detect the Ising-universality phase transitions, there have been proposed various quantifiers such as energy gap, fidelity susceptibility, and a number of variants of entanglement measures [37, 38]. As shown in the list, sophisticated quantifiers other than the energy gap play a significant role in recent studies. Correspondingly, a variety of simulation techniques, such as exact diagonalization (ED), density matrix renormalization group (DMRG), tensor product state (TPS), quantum Monte Carlo (QMC), and tensor network (TN) methods, have been employed. As presented, the exact diagonalization method is applicable to various types of quantifiers. So far, a limiting case $\eta = 1$ (Ising limit) has come under thorough investigation specifically, and the phase transition point h_c at this case $\eta = 1$ is shown for each study. As mentioned above, the overall features for generic η have not been investigated very extensively.

The rest of this paper is organized as follows. In the next section, we present the numerical results. The finite-size-scaling analysis is shown for $\eta = 1$, where preceding results are available. Then, similar analyses with η scaled are made with the crossover scaling theory. In Sec. 3, we address the summary and discussions.

Table 1 Related studies for the two-dimensional quantum XY model (3) are recollected. So far, a variety of techniques, such as exact diagonalization (ED), density matrix renormalization group (DMRG), tensor product state (TPS), quantum Monte Carlo (QMC), and tensor network (TN) methods, have been utilized successfully. As a probe to detect the underlying phase transition, there have been proposed a number of quantifiers such as energy gap, fidelity susceptibility, and a number of variants of entanglement measures [37,38]. As indicated, in almost all studies, the Ising limit $\eta = 1$ has been undertaken, and the phase transition point h_c at $\eta = 1$ is shown for each study.

method	quantifier	η range undertaken	$h_c _{\eta=1}$
ED [27]	energy gap	$\eta \leq 1$	3.05(1)
DMRG [32]	energy gap	$\eta = 1$	3.046
ED [33]	fidelity susceptibility	$\eta = 1$	2.95(1)
ED [34]	multipartite entanglement	$\eta = 1$	3.040
TPS [35]	entanglement measures	$\eta = 1$	3.25
QMC [12]	fidelity susceptibility	$\eta = 1$	3.0442(4)
TN [36]	bipartite entanglement per bond	$\eta \leq 1$	3.26
ED (this work)	fidelity susceptibility	$\eta \leq 1$	3.06(2)

2 Numerical results

In this section, we present the numerical results for the two-dimensional quantum XY model with a transverse magnetic field, Eq. (3). We employed the exact diagonalization method for the cluster with $N \leq 6 \times 6$ spins. We dwell on the Ising-universality branch, placing an emphasis on its multicriticality at $(h, \eta) = (2, 0)$.

As mentioned in Introduction, the multicriticality for the one-dimensional counterpart was studied with the fidelity susceptibility [20]. In this work [20], the authors took a direct route toward the multicritical point, setting the parameters like $h - h_c \sim \eta$. In this direct approach, the fidelity susceptibility peak splits into a series of sub-peaks, reflecting the intermittent level crossings [27] along the sector $\eta = 0$ ($h < h_c$). In this paper, in order to avoid such a peak splitting, we take a different approach to the multicritical point. We sweep the magnetic field h with $\eta (\neq 0)$ fixed to a certain constant value, and consider the multicritical singularity as a limiting case of the ordinary Ising universality class. To this end, we first consider the case $\eta = 1$, where a good deal of preceding results are available.

2.1 Scaling behavior for the fidelity susceptibility χ_F at the Ising limit $\eta = 1$

In this section, we make a finite-size-scaling analysis of the fidelity susceptibility for the fixed $\eta = 1$ (Ising limit); this scheme sets a basis for the subsequent crossover scaling analyses in Sec. 2.3.

To begin with, we recollect a number of formulas relevant to the present survey. According to Ref. [12], the fidelity susceptibility diverges as $\chi_F \sim L^{\alpha_F/\nu}$ at the critical point $h = h_c$, as the system size L enlarges. Here, the symbols, α_F and ν , denote the critical exponents for the correlation length

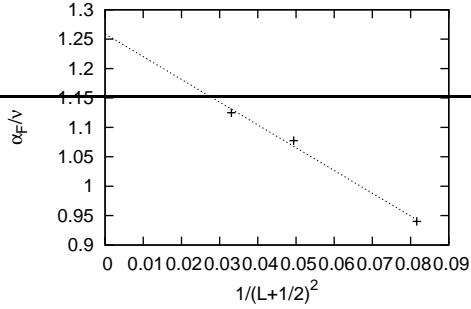


Fig. 3 The approximate critical exponent $\frac{\alpha_F}{\nu}(L, L+1)$ (4) is plotted for $1/(L + \frac{1}{2})^2$ with $\eta = 1$ and various system sizes $L = 3, 4, 5$. The least-squares fit to these data yields $\alpha_F/\nu = 1.259(20)$ in the thermodynamic limit $L \rightarrow \infty$. A possible systematic error is considered in the text.

and fidelity susceptibility, respectively; namely, the former (latter) diverges as $\chi_F \sim |h - h_c|^{-\alpha_F}$ ($\xi \sim |h - h_c|^{-\nu}$) in the vicinity of the critical point for sufficiently large L .

In Fig. 3, we present the approximate critical exponent

$$\alpha_F/\nu = \frac{\ln \chi_F(L+1)|_{h=h_c(L+1)} - \ln \chi_F(L)|_{h_c(L)}}{\ln(L+1) - \ln L}, \quad (4)$$

as a function of $1/(L + \frac{1}{2})^2$ with the fixed $\eta = 1$ and various system sizes $L = 3, 4, 5$; what is meant by the expression, $L + \frac{1}{2}$, in the abscissa scale is that the approximate critical exponent, $\frac{\alpha_F}{\nu}(L, L+1)$ (4), is calculated for a pair of system sizes, L and $L+1$, and the arithmetic mean, $L + \frac{1}{2}$, is taken as a representative value. Here, the approximate critical point $h_c(L)$ denotes χ_F 's peak position

$$\partial_h \chi_F(L)|_{h=h_c(L)} = 0, \quad (5)$$

for each L . The least-squares fit to the data in Fig. 3 yields an estimate $\alpha_F/\nu = 1.259(20)$ in the thermodynamic limit $L \rightarrow \infty$. As a reference, we carried out the similar analysis for a pair of data points, $L = 4$ and 5 , and arrived at an extrapolated value $\alpha_F/\nu = 1.221$. Regarding the deviation ≈ 0.038 from the above estimate 1.259 as a possible systematic error, we estimate the critical exponent as $\alpha_F/\nu = 1.259(38)$. Putting this estimate into the scaling relation [12]

$$\frac{\alpha_F}{\nu} = \frac{2}{\nu} - 2, \quad (6)$$

we arrive at the correlation-length critical exponent

$$\nu = 0.614(8). \quad (7)$$

Afterward, we make a comparison with the related studies.

We turn to the analysis of the critical point h_c . The approximate critical point $h_c(L)$ converges to the thermodynamic limit as $|h_c(L) - h_c| \sim 1/L^{1/\nu}$.

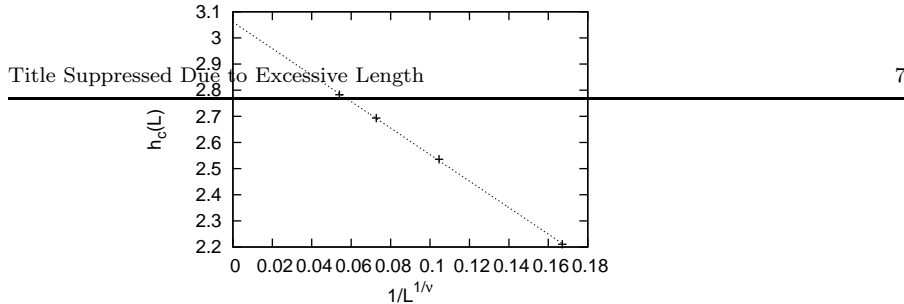


Fig. 4 The approximate critical point $h_c(L)$ (5) is plotted for $1/L^{1/\nu}$ with $\eta = 1$, $\nu = 0.614$ [Eq. (7)], and various system sizes $L = 3, 4, \dots, 6$. The least-squares fit to these data yields an estimate $h_c = 3.061(7)$ in the thermodynamic limit $L \rightarrow \infty$. A possible systematic error is considered in the text.

(This relation is anticipated from the above-mentioned formula $|h - h_c|^{-\nu} \sim \xi$ through the dimensional analysis.) In Fig. 4, we present the approximate critical point $h_c(L)$ as a function of $1/L^{1/\nu}$ with $\nu = 0.614$ [Eq. (7)], $\eta = 1$, and various system sizes $L = 3, 4, \dots, 6$. The least-squares fit to these data yields an estimate $h_c = 3.061(7)$ in the thermodynamic limit $L \rightarrow \infty$. As a reference, we carried out the similar analysis for a pair of data points, $L = 5$ and 6 , and arrived at an extrapolated value $h_c = 3.042$. Regarding the deviation ≈ 0.019 from the above estimate 3.061 as a possible systematic error, we estimate the critical point as

$$h_c = 3.06(2). \quad (8)$$

This is a good position to address an overview of the related studies for $\eta = 1$. By means of the fidelity-susceptibility-mediated analyses with the exact diagonalization method for $N \leq 20$ [33] and the quantum Monte Carlo simulation for $N \leq 48^2$ [12], the estimates, $(h_c, \nu) = (2.95(1), 0.7143)$ and $(3.0442(4), 0.625(3))$, respectively, were obtained. Our results, Eqs. (7) and (8), are comparable with these pioneering studies. By means of the exact diagonalization method for $N \leq 5^2$ with respect to the energy gap [27] and multipartite entanglement [34], there have been reported the results, $(3.05(1), 0.629(2))$ and $(3.040, 0.51)$, respectively. The former estimates were obtained by taking the weighted mean values for the simulation results performed at $\eta = 0.5, 0.7, 1.0$ under the periodic- and anti-periodic-boundary conditions independently. We stress that the present approach attains to admitting rather unbiased estimates with moderate computational effort. Similarly, via the density-matrix-renormalization-group [32], tensor-product-state [35], and tensor-network [36] methods, the estimates, $(h_c, \nu) = (3.046, 0.66)$, $h_c = 3.25$, and 3.26 , respectively, were obtained. Again, it is suggested that the fidelity-susceptibility-mediated scheme, albeit with the tractable system sizes restricted, yields unbiased estimates for the criticality.

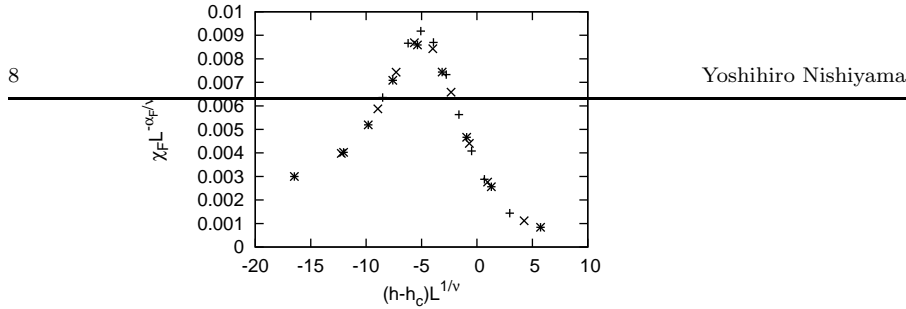


Fig. 5 The scaling plot, $(h - h_c)L^{1/\nu} - \chi_F L^{-\alpha_F/\nu}$, is presented for $\eta = 1$, $h_c = 3.06$ [Eq. (8)], $\nu = 0.614$ [Eq. (7)], $\alpha_F/\nu = 1.259$ [Eq. (6)], and various system sizes (+) $L = 4$, (x) 5, and (*) 6. The data collapse into a scaling curve, validating the finite-size-scaling analyses for the fidelity susceptibility.

2.2 Scaling plot for the fidelity susceptibility χ_F at the Ising limit $\eta = 1$

In this section, we present the scaling plot for the fidelity susceptibility, based on the finite-size-scaling formula [12]

$$\chi_F = L^x f((h - h_c)L^{1/\nu}), \quad (9)$$

with the scaling dimension $x = \alpha_F/\nu$ and a certain (non-universal) scaling function f .

In Fig. 5, we present the scaling plot, $(h - h_c)L^{1/\nu} - \chi_F L^{-\alpha_F/\nu}$, for $\eta = 1$ and various system sizes, $L = 4, 5, 6$; the symbol for each L is explained in the figure caption. Here, the scaling parameters, $h_c = 3.06$ [Eq. (8)], $\nu = 0.614$ [Eq. (7)], and $\alpha_F/\nu = 1.259$ [Eq. (6)], were determined in Sec. 2.1. The data in Fig. 5 seem to collapse into a scaling curve f satisfactorily, validating the consistency of the analyses in Sec. 2.1. In the next section, with η varied, the data are recast into an extended scaling formula, namely, the crossover scaling theory, so as to investigate the multicriticality at $(h, \eta) = (2, 0)$.

Last, we address a number of remarks. First, as presented in Fig. 5, the fidelity susceptibility exhibits a notable peak around the critical point. Actually, the scaling dimension α_F/ν of the fidelity susceptibility is larger than that of the specific heat α/ν because of the relation $\alpha_F/\nu = \alpha/\nu + 1$ between them. (This relation is derived from the hyper-scaling relation $\alpha = 2 - 3\nu$ together with Eq. (6).) The fidelity susceptibility has an advantage in that its enhanced singularity would dominate the regular (non-singular) part. Last, the fidelity susceptibility does not rely on any *ad hoc* assumptions for the order parameter involved. Such a feature is significant in the present study, because the crossover between the Ising- and XX -symmetric cases is our concern. Rather intriguingly, at the XX -symmetric point, the fidelity susceptibility exhibits even more pronounced peak (larger scaling dimension), as explained below.

2.3 Crossover scaling analyses for the fidelity susceptibility χ_F with η scaled

In this section, we carry out the crossover scaling analyses for the fidelity susceptibility around $\eta = 0$. Because in this case, an extra parameter η , which is supposed to converge to $\eta \rightarrow 0$ ($L \rightarrow \infty$), exists, the above-mentioned scaling formula (9) has to be extended. According to the crossover scaling theory [39, 40], the extended formula should read

$$\chi_F = L^{\dot{x}} g\left((h - h_c(\eta)) L^{1/\dot{\nu}}, \eta L^{\phi/\dot{\nu}}\right), \quad (10)$$

with the crossover exponent ϕ and a certain (non-universal) scaling function g ; the crossover exponent ϕ [39, 40] describes how the Ising universality for $\eta > 0$ turns into the end-point singularity at $\eta = 0$. As in Eq. (9), the indices, $\dot{x} = 3$ and $\dot{\nu} = 1/2$ [31, 41, 42], describe the singularities for the fidelity susceptibility and correlation length, respectively, right at the multicritical point $\eta = 0$. The former index $\dot{x} = 3$ is given by the scaling relation $\alpha_F/\nu = (\alpha + z\nu)/\nu$ [12] substituted with $\nu = 1/2$ [31, 41, 42], dynamical critical exponent $z = 2$ [31], and specific-heat critical exponent $\alpha = 1/2$; here, this index $\alpha = 1/2$ is read off from the first derivative of the magnetization $m \propto -\sqrt{h_c - h}$ [31] regarded as the internal energy.

As presented in Fig. 2, the crossover exponent ϕ determines the shape of the phase boundary in the vicinity of the multicritical point. Note that both arguments of the scaling function g in Eq. (10) should be dimensionless. Hence, the scaling dimensions for $h - h_c(\eta)$ and $\eta^{1/\phi}$ are identical, admitting the relation $h_c - h_c(0) \sim \eta^{1/\phi}$ [39, 40]. Therefore, the crossover scaling analysis has implications for the power-law singularity of the phase boundary.

We turn to the crossover-scaling analysis of the fidelity susceptibility, based on the above-mentioned formulas. In Fig. 6, we present the crossover scaling plot, $(h - h_c(\eta))L^2 - \chi_F L^{-3}$, for various system sizes, $L = 4, 5, 6$; the symbol for each L is explained in the figure caption. Here, the second argument of the scaling function g (10) is fixed to a constant value $\eta L^{2\phi} = 10.8$ with $\phi = 1$, and the critical point h_c was determined through the same scheme as that of Sec. 2.1 by using the index $\nu = 0.63002$ [43]. The crossover-scaled data in Fig. 6 seem to collapse into a scaling curve satisfactorily. Actually, the data for (\times) $L = 5$ and ($*$) $L = 6$ almost overlap each other, entering at the crossover-scaling regime. Such a feature strongly supports the proposition $\phi = 1$.

Similar analyses were made for various values of ϕ . In Fig. 7, we present the crossover scaling plot, $(h - h_c(\eta))L^2 - \chi_F L^{-3}$, for the system sizes, $L = 4, 5, 6$, with the fixed $\eta L^{2\phi} = 26.5$ under postulating $\phi = 1.25$. The crossover-scaled data get scattered, as compared to those of Fig. 6; particularly, the right-side slope displays notable dispersion of the data, whereas the left hand side shows an alignment. Additionally, in Fig. 8, we present the crossover scaling plot, $(h - h_c(\eta))L^2 - \chi_F L^{-3}$, for various system sizes, $L = 4, 5, 6$, with fixed $\eta L^{2\phi} = 4.4$ under setting $\phi = 0.75$. For such a small ϕ , on the contrary, the left-side-slope data around $(h - h_c)L^2 \approx -10$ become dissolved, whereas the right hand side shows a tolerable overlap. Hence, we conclude that the

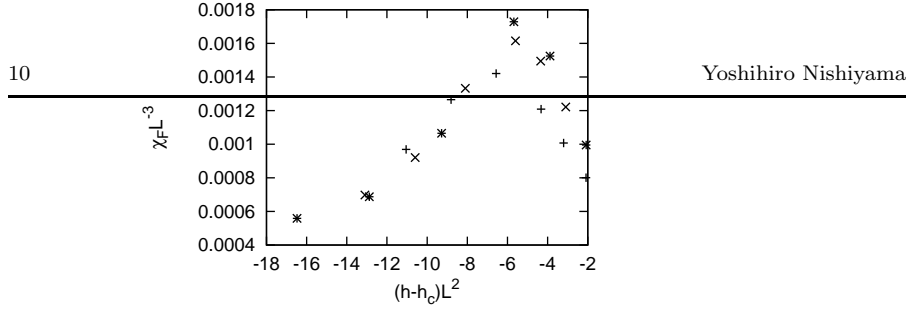


Fig. 6 The crossover scaling plot, $(h-h_c)L^2-\chi_F L^{-3}$, is presented for various system sizes (+) $L = 4$, (\times) 5, and (*) 6 with the fixed $\eta L^{2\phi} = 10.8$ (second argument of the crossover scaling function g (9)) under setting $\phi = 1$. The crossover-scaled data collapse into a scaling curve, supporting $\phi = 1$.

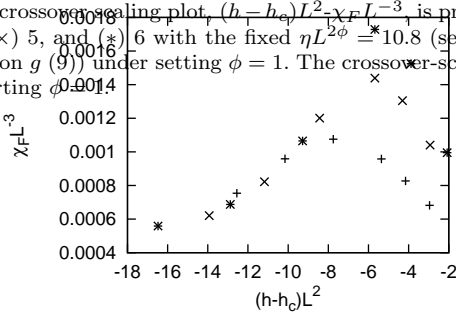


Fig. 7 The crossover scaling plot, $(h-h_c)L^2-\chi_F L^{-3}$, is presented for various system sizes (+) $L = 4$, (\times) 5, and (*) 6 with the fixed $\eta L^{2\phi} = 26.5$ (second argument of the crossover scaling function g (9)) under postulating $\phi = 1.25$. The right-side-slope data get scattered, as compared to those of Fig. 6.

crossover critical exponent locates within

$$\phi = 1.0(2). \quad (11)$$

This result indicates that the phase boundary increases, at least, monotonically with the anisotropy η .

A number of remarks are in order. First, the fidelity susceptibility exhibits a notable peak around the multicritical point. As noted above, the scaling dimension $\hat{x} = 3$ at the multicritical point is even larger than that of the Ising-universality transition $x \approx 1.2 \dots$. Hence, the underlying mechanism behind the crossover scaling plot, Fig. 6, differs from that of the Ising-universality transition, Fig. 5. In this sense, the overlap of the scaling plot, Fig. 6, is by no means coincidental, and rather it requires the exponent ϕ to be finely adjusted. Last, the fidelity susceptibility is applicable to both Ising- and XX -symmetric cases. Actually, according to Ref. [9], the fidelity susceptibility detects the first-order phase transitions, and the (putative) critical exponents make sense.

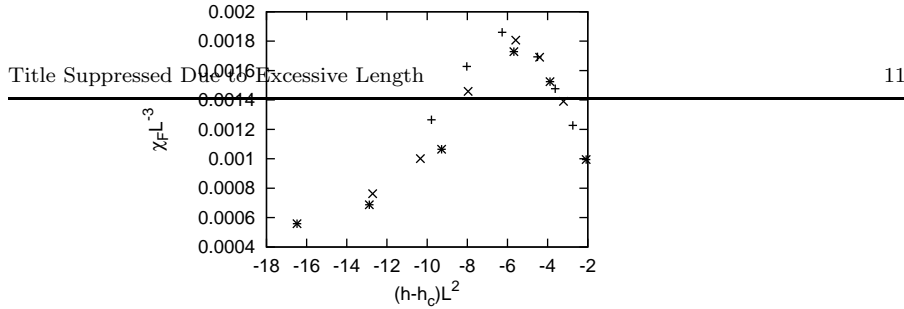


Fig. 8 The crossover scaling plot, $(h - h_c)L^2 - \chi_F L^{-3}$, is presented for various system sizes (+) $L = 4$, (\times) 5 , and ($*$) 6 with the fixed $\eta L^{2\phi} = 4.4$ (second argument of the crossover scaling function g (9)) under postulating $\phi = 0.75$. The left-side-slope data around $(h - h_c)L^2 \approx -10$ become dissolved, as compared to those of Fig. 6.

Our study owes the initial settings for the multicritical indices, $\dot{x} = 3$ and $\dot{\nu} = 1/2$, to this recent development [9].

3 Summary and discussions

The two-dimensional quantum XY model with a transverse magnetic field (3) was investigated numerically. We dwell on the Ising-universality branch, placing an emphasis on the multicriticality at $(h, \eta) = (2, 0)$, where a slowing down [30] affects the efficiency of the quantum Monte Carlo simulations. By means of the exact diagonalization method, we calculated the fidelity susceptibility in order to detect the phase transitions. With fixed $\eta = 1$ (Ising limit), the finite-size-scaling analysis of the fidelity susceptibility was made, and the results are in agreement with those of the preceding studies. Thereby, with η scaled, the crossover scaling analysis was made, and it turned out that the data are cast into the crossover scaling formula (10) rather satisfactorily. As a consequence, we estimate the crossover exponent as $\phi = 1.0(2)$. The preceding exact diagonalization analysis [27] indicates a “monotonous” [29] dependence of $h_c(\eta)$ on η . Supporting this claim, our result $\phi = 1.0(2)$ strongly suggests a linear increase of $h_c(\eta)$ with η .

In regard to the reentrant scenario [29] advocated for the spin-anisotropic spherical model, it would be intriguing to investigate the systems with the extended internal symmetries such as the spin- $S = 1$ XY chain [44], and the two-band Hubbard model [45]. Actually, the latter exhibits a curved phase boundary (see Fig. 10 of Ref. [45]) reminiscent of the reentrant scenario. This problem will be left for the future study.

Author contribution statement

Y.N. conceived the presented idea, and carried out the numerical simulations. He analyzed the simulation results, and wrote up the manuscript.

References

1. A. Uhlmann, Rep. Math. Phys. **9** (1976) 273.
2. R. Jozsa, J. Mod. Opt. **41** (1994) 2315.
3. A. Peres, Phys. Rev. A **30** (1984) 1610.
4. T. Gorin, T. Prosen, T. H. Seligman, and M. Žnidarič, Phys. Rep. **435** (2006) 33.
5. H. T. Quan, Z. Song, X. F. Liu, P. Zanardi, and C. P. Sun, Phys. Rev. Lett. **96** (2006) 140604.
6. P. Zanardi and N. Paunković, Phys. Rev. E **74** (2006) 031123.
7. H.-Q. Zhou, and J. P. Barjaktarevič, J. Phys. A: Math. Theor. **41** (2008) 412001.
8. W.-L. You and Y.-L. Dong, Phys. Rev. B **84** (2011) 174426.
9. D. Rossini and E. Vicari, Phys. Rev. E **98** (2018) 062137.
10. V. R. Vieira, J. Phys: Conference Series **213** (2010) 012005.
11. S.-J. Gu, Int. J. Mod. Phys. B **24** (2010) 4371.
12. A. F. Albuquerque, F. Alet, C. Sire, and S. Capponi, Phys. Rev. B **81** (2010) 064418.
13. D. Schwandt, F. Alet, and S. Capponi, Phys. Rev. Lett. **103** (2009) 170501.
14. C. De Grandi, A. Polkovnikov, and A. W. Sandvik, Phys. Rev. B **84** (2011) 224303.
15. L. Wang, Y.-H. Liu, J. Imriška, P. N. Ma, and M. Troyer, Phys. Rev. X **5** (2015) 031007.
16. J. Zhang, X. Peng, N. Rajendran, and D. Suter, Phys. Rev. Lett. **100** (2008) 100501.
17. M. Kolodrubetz, V. Gritsev, and A. Polkovnikov, Phys. Rev. B **88** (2013) 064304.
18. S.-J. Gu and W. C. Yu, Europhys. Lett. **108** (2014) 20002.
19. Q. Luo, J. Zhao, and X. Wang, Phys. Rev. E **98** (2018) 022106.
20. V. Mukherjee, A. Polkovnikov, and A. Dutta, Phys. Rev. B **83** (2011) 075118.
21. J. Maziero, H. C. Guzman, L. C. Céleri, M. S. Sarandy, and R. M. Serra, Phys. Rev. A **82** (2010) 012106.
22. Z.-Y. Sun, Y.-Y. Wu, J. Xu, H.-L. Huang, B.-F. Zhan, B. Wang, and C.-B. Duanpra, Phys. Rev. A **89** (2014) 022101.
23. G. Karpat, B. Çakmak, and F. F. Fanchini, Phys. Rev. B **90** (2014) 104431.
24. S. Katsura, Phys. Rev. **127** (1962) 1508.
25. E. Barouch, B. M. McCoy, and M. Dresden, Phys. Rev. A **2** (1970) 1075.
26. M. Suzuki, Progress Theor. Phys. **46** (1971) 1337.
27. M. Henkel, J. Phys. A: Mathematical and Theoretical **17** (1984) L795.
28. S. Jalal, R. Khare, and S. Lal, arXiv:1610.09845.
29. S. Wald and M. Henkel, J. Stat. Mech.: Theory and Experiment (2015) P07006.
30. V. Z. Kashurnikov, N. V. Prokof'ev, B. V. Scistunov, and M. Troyer, Phys. Rev. B **59** (1999) 1162.
31. V. Zapf, M. Jaime, and C.D. Batista, Rev. Mod. Phys. **86** (2014) 563.
32. M. S. L. du Croo de Jongh and J.M.J. van Leeuwen, Phys. Rev. B **57** (1998) 8494.
33. W.-C. Yu, H.-M. Kwok, J. Cao and S.-J. Gu, Phys. Rev. E **80** (2009) 021108.
34. A. Montakhab and A. Asadian, Phys. Rev. A **82** (2010) 062313.
35. C.-Y. Huang and F.-L. Lin, Phys. Rev. A **81** (2010) 032304.
36. B. Braierr-Orrs, M. Weyrauch, and M. V. Rakov, Quantum Information and Computation **16** (2016) 0885,
37. L. Amico, R. Fazio, A. Osterloh, and V. Vedral, Rev. Mod. Phys. **80** (2008) 517.
38. R. Horodecki, P. Horodecki, M. Horodecki, and K. Horodecki, Rev. Mod. Phys. **81** (2009) 865.
39. E.K. Riedel and F. Wegner, Z. Phys. **225** (1969) 195.
40. P. Pfeuty, D. Jasnow, and M. E. Fisher, Phys. Rev. B **10** (1974) 2088.
41. M. Adamski, J. Jędrzejewski, and T. Krokhumalskii, arXiv:1502.05268.
42. C. Hoeger, G. V. Gehlen, and V. Rittenberg, J. Phys. A: Math. Gen. **18** (1985) 1813.
43. M. Hasenbusch, Phys. Rev. B **82** (2010) 174433.
44. W. Hofstetter and M. Henkel, J. Phys. A: Math. Gen. **29** (1996) 1359.
45. C. De Franco, L. F. Tocchio and F. Becca, Phys. Rev. B **98** (2018) 075117.